Chemical Engineering Journal 433 (2022) 134607

Contents lists available at ScienceDirect

Chemical Engineering Journal

journal homepage: www.elsevier.com/locate/cej

Dynamic CO_2 sorption on MgO-based sorbent in the presence of CO and H_2O at elevated pressures

Gina Bang [a], Kyung-Min Kim [b], Seongmin Jin [a,c,*], Chang-Ha Lee [a,*]

[a] Department of Chemical and Biomolecular Engineering, Yonsei University, Seoul 03722, Korea
[b] Department of Biochemical Engineering, Gangneung-Wonju National University, Gangneung 25457, Korea
[c] Institute of Chemical Sciences and Engineering, École Polytechnique Fédérale de Lausanne (EPFL), Lausanne, Switzerland

ARTICLE INFO

Keywords:
CO_2 sorption
Sorption mechanism
MgO
Breakthrough experiments
In situ DRIFTS

ABSTRACT

The presence of gas species other than the target adsorbate in practical conditions causes complications in implementing a sorption-based process because of synergistic or detrimental effects on the sorption mechanism. MgO-based sorbents have attracted massive attention for the pre-combustion CO_2 capture, where H_2O and CO co-exist in emission gas. Although H_2O has been reported to greatly enhance CO_2 sorption kinetics, CO_2 sorption behavior and mechanism under a large quantity of H_2O as in the practical condition remain unclear. Furthermore, CO_2 sorption behavior in the presence of CO has not been adequately examined. Here, the dynamic CO_2 sorption behavior of MgO-based sorbent was understood by coupling the breakthrough experiment under practically relevant conditions with *in situ* DRIFTS results. At elevated pressures, the sorption performance was considerably enhanced, whereas the influence by temperatures was insignificant. In addition, H_2O enhanced CO_2 sorption kinetics and initial CO_2 sorption on MgO-based sorbent, whereas CO hindered them. *In situ* DRIFTS analyses for the mechanism study revealed that OH groups generated from H_2O dissociation created highly basic sites that promoted the formation of monodentate carbonate, thereby enhancing the initial CO_2 sorption. In contrast, CO hampered CO_2 sorption through two mechanisms: (1) competitive sorption between CO_2 generated from the water–gas shift reaction and CO_2 in the feed; (2) interference of the promoted sorption by the molten nitrate salts. This study demonstrated that the practical condition of the pre-combustion CO_2 capture significantly alters the CO_2 sorption behavior of MgO, thereby providing insights for the ultimate implementation of MgO-based sorbents.

1. Introduction

Energy generated from fossil fuels accounts for 80 % of the total energy demand and the emission of carbon dioxide (CO_2) therein is deteriorating the climate changes [1]. Therefore, the International Energy Agency (IEA) has proposed global CO_2 emission reduction policies that involve increasing the proportion of carbon capture, utilization, and storage (CCUS) technologies to 21.2 % by 2070 to achieve zero CO_2 emission [1]. In order to meet this target and facilitate more sustainable fossil fuel use, carbon capture technologies need to be developed further for their ultimate application [2]. Of these technologies, sorption technology is advantageous because of its wide temperature and pressure operation window and its application of environmentally friendly materials [3]. Therefore, many advanced solid sorbents are being developed for pre-combustion and/or post-combustion CO_2 capture [4].

In the natural gas combined cycle (NGCC) or integrated gasification combined cycle (IGCC) processes for power generation [5], the pre-combustion CO_2 capture can be implemented after a water–gas shift (WGS) reactor, where H_2 and CO_2 are generated at high pressures (2–7 MPa) and intermediate temperatures (180–550 °C) by a reaction between CO and H_2O [6]. Owing to these relatively high temperatures, CaO and MgO-based sorbents, which can chemically capture CO_2, are being developed [7,8]. The temperature regime for CO_2 sorption and regeneration of MgO (200–450 °C) closely aligns with the temperature range of the effluent gas from WGS reactors; therefore, the research on MgO has been particularly conducted, leading to recent advancements in CO_2 capture performance [9–11]. Of the various approaches, utilizing alkali metal salts along with MgO has been shown to promote the sorption capacity of MgO and notably enhance the rate of CO_2 sorption [12,13]. Therefore, the research on MgO-based sorbents has been

* Corresponding authors.
E-mail addresses: seongmin.jin@epfl.ch (S. Jin), leech@yonsei.ac.kr (C.-H. Lee).

https://doi.org/10.1016/j.cej.2022.134607
Received 22 November 2021; Received in revised form 5 January 2022; Accepted 6 January 2022
Available online 10 January 2022

focused on optimizing the types and proportions of alkali metal salts, investigating the sorption mechanism, and examining the roles of alkali nitrates and carbonates [14–16].

Even after considerable advances in MgO-based sorbents with enhanced CO_2 capture performances, their ultimate application requires a better understanding of the dynamic sorption behavior in a fixed bed as well as under more realistic conditions including low CO_2 concentration, high amounts of H_2O (~30 %), the presence of CO, and high pressures. A thermogravimetric analysis (TGA) is widely used to evaluate the performances of CO_2 sorbents because it efficiently screens best-performing sorbents and facilitates long-term stability tests. Recent studies using the TGA method have revealed that a small amount of H_2O can promote CO_2 sorption, and low partial pressure of CO_2 is unfavorable for its sorption [17,18]. However, TGA is limited because it cannot be used when closely simulating the effluent gas of WGS reactors [19,20]. In this regard, performance evaluation in a fixed bed can further the understanding of dynamic sorption behavior under more practical gas compositions, enabling efficient reactor design. In particular, non-target gas species such as H_2O and CO can affect the sorption of CO_2 on the surface of MgO-based sorbents; therefore, a clear understanding of their effects on CO_2 sorption is possible through a fixed bed study using gas compositions close to those in practical conditions.

Studying the sorption mechanism in the presence of non-target gas species can also facilitate the design of efficient MgO-based sorbents. However, utilizing alkali metal salts to promote the capacities of MgO-based sorbents complicates the mechanistic study of CO_2 sorption. Therefore, most studies have focused on examining the role of alkali metal salts using *in situ* analyses under the flow of pure CO_2 or a mixture of CO_2 and inert gases. A recent study has revealed the correlation between the solubility of MgO in nitrate salts and the carbonation of MgO, from an ion dynamics perspective [21]. For the nitrate salts-based promotion of sorption, the formation of a nitrite intermediate in the cyclic reaction between CO_2 and nitrate has been reported [22]. However, no information is available about the effects of non-target gas species on CO_2 sorption due to the complexity to include H_2O and CO in the sorption system.

In this study, dynamic CO_2 sorption behavior of an MgO-based sorbent was observed in various practically relevant conditions by controlling the temperature, pressure, and feed composition. And the effects of non-target gas species such as H_2O and CO on CO_2 sorption were also studied. To achieve these goals, the study had to be conducted in a fixed bed using more real gas compositions, and the pelletized sorbent was essential to avoid the pressure drop and sorbent loss in the sorbent bed. This study selected spherically structured $MgCeO_x$ sorbent with alkali metal salt promoters, which showed much higher CO_2 capture performance than powder MgO sorbent [9], was packed in a fixed bed. And its CO_2 capture performance was examined. *In situ* DRIFTS revealed that the non-target gas species can considerably affect the CO_2 sorption mechanism, thereby enabling the interpretation of the dynamic sorption behavior. This systematic evaluation and the following mechanistic study in the presence of non-target gas species can help overcome practical obstacles for designing CO_2 sorbents and facilitate the ultimate utilization of MgO-based sorbents not only for CO_2 capture but also for sorption-enhanced reaction.

2. Material and methods

2.1. Sorbent synthesis

The $MgCeO_x$ composite was prepared using a sol–gel combustion-assisted method described in the previous study [9]. For the synthesis of the $MgCeO_x$, 2.56 g of magnesium nitrate hexahydrate (Signa-Aldrich, India; 99 %), 0.43 g of cerium nitrate hexahydrate (Sigma-Aldrich, France; 99 %), and 4.62 g of citric acid monohydrate (Sigma-Aldrich, USA; 98 %) were dissolved in 11.9 ml of deionized water (Daejung, Korea, HPLC grade). The molar ratios of citric acid and water to total metals (Mg and Ce) were fixed at 2 and 60, respectively, with the molar ratio of Ce to Mg set to 0.1. The solution mixture was stirred in an oil bath at 80 °C for 5 h and then dried in an oven at 90 °C for 4 h. The dried sample was ground and then dried again at 110 °C overnight. Subsequently, the dried sample was calcined using the two-step method in a tube furnace to obtain a structured bead morphology and high surface area [23]. Firstly, the temperature was ramped up to 150 °C at a rate of 1 °C/min and maintained at 150 °C for 9 h. Subsequently, the temperature was ramped up again from 150 °C to 450 °C at the rate of 1 °C/min and then maintained at 450 °C for 10 *h*. After calcination, the obtained samples were sieved (mesh size, 250 μm).

Table 1
Summary of experimental parameters for TGA and breakthrough experiments.

Figure number	Feed gas composition [vol.%]				Temperature [°C]	Pressure [bar]
	CO_2	H_2O	CO	Ar		
S4	30	0	0	balanced	300/ 325/ 350	1
1(a)	30	30	0	balanced	300/ 325/ 350	1
1(b)	30	0/ 30/ 60	0	balanced	300	1
2(a)	30	30	0	balanced	300	1/ 3/ 6/ 10
2(b)	30	30	0/ 1/ 5	balanced	300	10
S6	0	30	5	balanced	300	10

The salt-promoted $MgCeO_x$ sorbent was prepared by wet mixing the $MgCeO_x$ composite and alkali metal salt solution [9]. $LiNO_3$ (Sigma-Aldrich, Germany; 99 %), $NaNO_3$ (Daejung, Korea; 99.0 %), Na_2CO_3 (Sigma-Aldrich, USA; 99.5%), and K_2CO_3 (Duksan, Korea; 99.0 %) were used to prepare the alkali metal salt solution. The molar ratio of the alkali metal salts to the Mg was fixed at 0.17; the molar ratio of the alkali metal salts was fixed as $LiNO_3$:$NaNO_3$:Na_2CO_3:K_2CO_3 = 0.2:0.76:0.04:0.5. It was reported that CO_2 sorption capacity can be improved to the largest extent by $NaNO_3$ among nitrate salts [24]. Therefore, to maximize CO_2 sorption by using nitrate salts, the melting point (or eutectic point) of a nitrate mixture including $NaNO_3$ should be close to the target temperature of CO_2 sorption. In this study, $LiNO_3$ was used to reduce the eutectic melting point of the nitrate salt mixture in the CO_2 sorption process whereas $NaNO_3$ was used to maximize the enhancement of the CO_2 sorption capacity.

The solution was stirred at 200 rpm for 3 h and at 100 rpm for 1 h at 60 °C, and then dried overnight in an oven at 80 °C. After drying, the resultant sample was calcined by ramping up the temperature to 450 °C at a heating rate of 1 °C/min, and then sieved (mesh size, 250 μm). The distribution of salts in the as-prepared $MgCeO_x$ sorbent was observed via field-emission scanning electron microscopy (FE-SEM; JEOL-7610F-Plus, JEOL) and elemental mapping via energy-dispersive X-ray spectroscopy (EDS; X-MAX TSR, OXFORD Instruments).

2.2. Evaluation of CO_2 sorption performance

The CO_2 sorption performance of the salt-promoted $MgCeO_x$ was evaluated using both TGA and breakthrough experiments. Since the samples were prepared from different batches, the reproducibility of the as-prepared samples for CO_2 capture performance was confirmed via the TGA experiments. The operating conditions used for the CO_2 sorption tests are listed in Table 1.

2.2.1. Thermogravimetric analysis (TGA) experiments

Thermogravimetric analysis (TGA; TGA 4000, Perkin Elmer) was used to examine the sorption behavior of the salt-promoted $MgCeO_x$. The capacities and rates of CO_2 sorption were estimated from the CO_2 uptake curves. 15 mg of the prepared sample was loaded into an alumina crucible, and pre-treated at 450 °C for 30 min under a flow of 40 ml/min

Table 2
Summary of feed gas compositions for *in situ* DRIFTS experiments[a].

Gas condition	Feed gas composition [vol.%]			
	CO_2	H_2O	CO	Ar
Dry CO_2	30	–	–	70
Wet CO_2	30	10	–	60
Wet CO_2/CO	30	10	5	55
Wet CO	–	10	5	85
Dry CO	–	–	5	95

[a] All the *in situ* DRIFTS experiments were conducted at 300 ℃, 1 bar, and 50 ml/min.

of N_2 and a heating rate of 20 °C/min to remove any adsorbed gases. Thereafter, the CO_2 uptake experiments were conducted at various target temperatures (300, 325, and 350 °C) and a CO_2 flow of 40 ml/min at a pressure of 1 bar.

2.2.2. Breakthrough experiments

Fig. S1 depicts a fixed-bed reactor system that was used to conduct CO_2 breakthrough experiments for various feed conditions. 0.7 g of salt-promoted $MgCeO_x$ was packed in a column with an inner diameter of 7.7 mm, and both ends were fixed with quartz wool. A thermocouple was inserted into the packed column to measure the temperature of the packed sorbent layer. The feed gases comprised CO_2, CO, H_2O, and Ar balanced in different ratios, as presented in Table 1. H_2O was supplied using a high-performance liquid chromatography pump (HPLC pump; Lab Alliance Series I). The feed mixture was fed into a coiled preheater. In order to prevent the condensation of the generated water vapor, the temperature of the column and the lines were maintained at 250 °C using heating tapes.

The sorbent was pre-treated by purging with He at 450 °C for 30 min. Subsequently, breakthrough experiments were conducted at the desired temperatures (300, 325, and 350 °C) with a feed gas flow of 42 ml/min. Experimental pressures were controlled at 1, 3, 6, and 10 bars using a back pressure regulator (BPR; Bronkhorst High-tech). In order to ensure stable water vapor production, the humidity was monitored with a humidity detector (Dew point thermometer hygrometer; Traceable Products) operating at the high temperature and pressure, which was installed prior to the BPR, using a bypass line. Before performing the breakthrough experiments, the desired content of H_2O was confirmed on the detector. The product gas was analyzed via an online mass spectrometer (MS; HPR 20, Hidden Analytical Ltd.), after removing the water vapor with a cold trap. The signal-to-noise ratio of the MS was 1250 (error range of 0.08 %).

The water removal was also confirmed by another humidity detector, after the BPR. The product gases were quantified using multivariate calibration for mass spectrometry because of interfering gases, *i.e.,* CO primary peak and CO_2 secondary peak, having similar MS peak locations at *m/z* of 28 [25].

2.3. In situ DRIFTS experiments

In order to investigate the CO_2 sorption process of salt-promoted $MgCeO_x$ in the presence of H_2O and CO, *in situ* diffuse reflectance infrared Fourier-transformed spectroscopy (DRIFTS; Nicolet iS10, Thermo Scientific) was used. The signal-to-noise ratio of the IR analyzer was 50,000 (error range of 0.002 %) and the spectral resolution was 0.25 cm^{-1}. The sample was prepared by mixing the salt-promoted $MgCeO_x$ and KBr at a mass ratio of 1:3 and dried in an oven at 60 °C for 1 h. Before each measurement, the dried samples were pretreated with Ar at a flow rate of 50 ml/min at 450 °C for 30 min using the DRIFTS cell equipped with Zn-Se windows. After the pre-treatment, the samples were exposed to different compositions of the feed streams at a flowrate of 50 ml/min at 300 °C for 30 min. The feed composition used for each experiment and their corresponding names are summarized in Table 2 and denoted with a capitalized first letter such as Dry and Wet. A bubbler was installed to supply H_2O to the feed gas before it enters the DRIFTS cell, as presented in Fig. S2. The water vapor content in the feed gas was measured using the humidity detector. Spectral data were collected in the range of 4000 ~ 750 cm^{-1} using a mercury cadmium telluride (MCT) cryodetector.

2.4. CO_2/CO pulse titration experiments

The CO_2/CO pulse titration experiment was designed and conducted using a ChemBET Pulsar TPR/TPD unit (Quantachrome) to confirm the competitive CO chemisorption with CO_2. 0.05 g of salt-promoted $MgCeO_x$ sorbent was loaded into a U-shaped quartz cell and pre-treated at 450 °C for 30 min under a flow of 40 ml/min of He. Then, the pre-treated sorbent was cooled down to 300 °C with He purge flow. Afterward, 300 μl of gas (CO or CO_2) was introduced through a six-way valve for every injection and the interval time between two adjacent injections was maintained at 90 min to avoid an overlap between injections. The gas profile was measured by MS, and the following three experiments were performed under different conditions.

(i) Pulse I: CO_2 pulse was injected to the pre-treated sample.
(ii) Pulse II: CO pulse was injected to the pre-treated sample.
(iii) Pulse III: CO_2 pulse was injected after 4 h of He purge to the CO-treated sample in Pulse II experiment.

3. Results and discussion

The spherically structured $MgCeO_x$ composite was obtained using

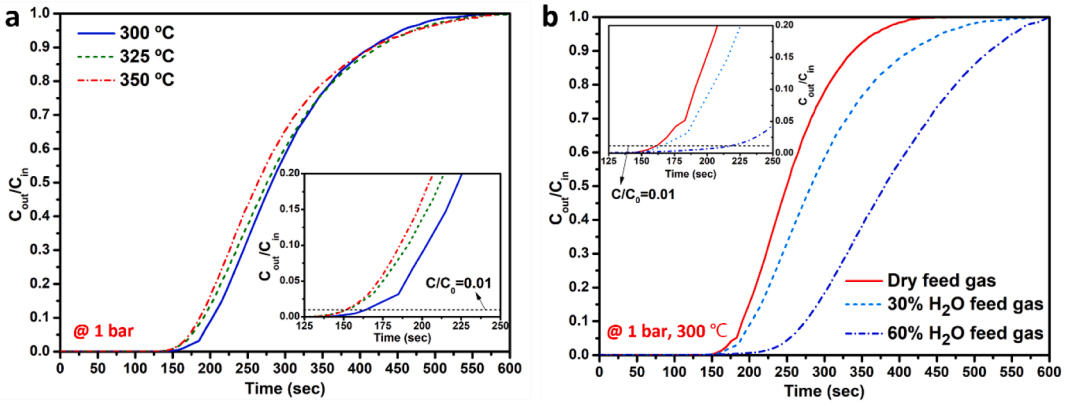

Fig. 1. CO_2 breakthrough curves (a) at different temperatures under the flow of 30 vol.% CO_2, 30 vol.% H_2O, and balance Ar and (b) at 300 °C with different H_2O compositions and fixed 30 vol.% CO_2 and balance Ar. (The black dotted line in the inset represents $C/C_0 = 0.01$ as the breakthrough time).

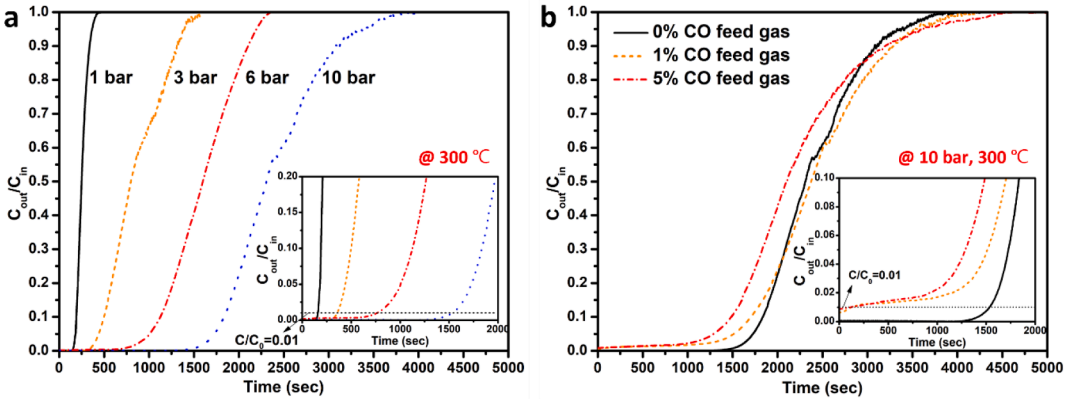

Fig. 2. CO_2 breakthrough curves at (a) different pressure conditions and (b) different CO compositions. (The feed gas composition in Fig. 2(a) was 30 vol.% CO_2, 30 vol.% H_2O, and balance Ar. In Fig. 2(b), the composition of CO_2 and H_2O was fixed, and the concentration of CO was varied with balanced Ar as presented in Table 1).

the sol–gel combustion-assisted method. A detailed study on the morphology of $MgCeO_x$ composite was performed in the previous study [9]. Additionally, it was confirmed that the salts in the salt-promoted $MgCeO_x$ sorbent were evenly dispersed via elemental mapping images (Fig. S3).

Before conducting breakthrough experiments, the reproducibility of as-synthesized samples was tested via the CO_2 uptake curves of TGA test because the samples were prepared from different batches even at the same preparation condition. The reproducibility of CO_2 capture capacity was confirmed within less than ± 2 %.

3.1. *Dynamic CO_2 sorption behavior under practically-relevant conditions*

TGA and breakthrough experiments were performed to examine the CO_2 sorption behavior of the salt-promoted $MgCeO_x$ in various conditions (Table 1). Whereas pure CO_2 was used in TGA tests, the breakthrough experiments enabled to test sorption behavior at lower CO_2 concentration (30 vol.%) with and without water vapor (Table 1). The breakthrough time in this study was determined as the time, where C/C_0 is 0.01, indicated by the black horizontal dotted line in Fig. 1.

The temperature dependency of the CO_2 sorption behavior was initially evaluated. Compared to the considerable decrease in the CO_2 sorption capacity and kinetic with increasing temperatures in the TGA tests (Fig. S4), the shapes of the breakthrough curves were similar at 300, 325, and 350 °C; however, the breakthrough time was shortened as the temperature increased (164, 152, and 151 secs, respectively) (Fig. 1(a)).

A decrease in CO_2 sorption kinetics of salt-promoted MgO-based sorbents is generally observed above a certain temperature [17,26]. The mechanism of enhanced CO_2 sorption in alkali metal nitrate salts-promoted MgO is based on the phase transition of nitrate salts to molten state above its melting temperature, where the dissolution of CO_2 and MgO into molten nitrate salts can be facilitated [21,22,27]. On the other hand, further temperature increase above the melting temperature results in decreasing CO_2 solubility as well as preventing $MgCO_3$ formation due to its exothermic reaction [28]. Therefore, an optimal temperature for CO_2 sorption kinetics exists, which depends on the composition and eutectic point of alkali metal nitrate mixtures. At the ratio of nitrate salts used in this study ($LiNO_3/NaNO_3 = 0.2$), the melting temperature of nitrate salt mixture is 275 °C, which is lower than the CO_2 sorption temperatures, *i.e.*, 300, 325, and 350 °C. Therefore, the decrease of CO_2 sorption capacity and kinetics with increasing temperature in Fig. S4 agreed with the previous studies.

On the contrary, it was noted that the temperature dependency of breakthrough curves was not as prominent as CO_2 uptake curves. This result indicated that the dynamic sorption behavior in the fixed bed could be fairly different from that observed in TGA analysis because the residence time (contact time) of gas in the sorbent bed was limited in the breakthrough experiments. The similar pattern of the breakthrough curves implies similar sorption mechanism regardless of the applied temperature. Reduction in the breakthrough time with increasing temperature has been reported in physisorption [29]. However, CO_2 sorption in the salt-promoted MgO at intermediate temperatures includes both physisorption and chemisorption; therefore, a more detailed mechanism study was required.

In the WGS reactor, of which effluent gas can be introduced to the pre-combustion CO_2 capture unit, a high ratio of steam (H_2O) to carbon (CO) is preferred to prevent the carbon deposition on the catalyst in the WGS reactor [30]. In this regard, the water content of the effluent gas from the WGS reactor can be modulated depending on the reaction conditions. Therefore, the effect of water vapor on the dynamic CO_2 sorption behavior was investigated by varying the content of water vapor from 0 to 60 % (Fig. 1(b)).

The breakthrough times for dry feed, 30 % H_2O feed, and 60 % H_2O feed gases were 159, 164, and 213 sec, respectively. CO_2 capture performance in the presence of 30 % H_2O was not as significantly enhanced as that observed in the TGA results of the previous study [17], where only 2.5 vol.% of water vapor considerably promoted the sorption kinetics. However, when the water content was further increased to 60 %, the breakthrough time was increased to 213 sec and the sorption capacity was greatly enhanced.

The shapes of the breakthrough curves under the wet feed conditions were similar to each other, indicating a similar sorption mechanism. However, the breakthrough curve for the dry feed condition was slightly steeper than the curves in the presence of water vapor. In the case of the physisorption, non-target species in the feed gas typically cause a reduction in the sorption capacity of the target gas, thereby widening the breakthrough curve's shape because of competitive adsorption [31]. However, Fig. 1(b) indicates that H_2O is likely to participate in CO_2 sorption on the salt-promoted $MgCeO_x$ through chemisorption. Moreover, these results emphasized that understanding the sorption behavior is crucial in developing sorbents for practically relevant conditions.

The total pressure of effluent gas from the WGS reaction is in the range of 20 to 70 bars [6]; however, the difficulty in operating at high pressure in the presence of water vapor hindered studying the potential of MgO-based sorbent at high pressure. Therefore, the effect of pressures on CO_2 capture was preliminarily investigated under wet feed gas (Table 1) from 1 to 10 bars, as presented in Fig. 2(a). Since all breakthrough experiments were performed with the same feed flow rate (42 ml/min at STP), increasing the pressure resulted in longer residence time in the bed. In order to exclude the effect of low linear velocity inside the reactor at high pressures on the breakthrough time, when Ar

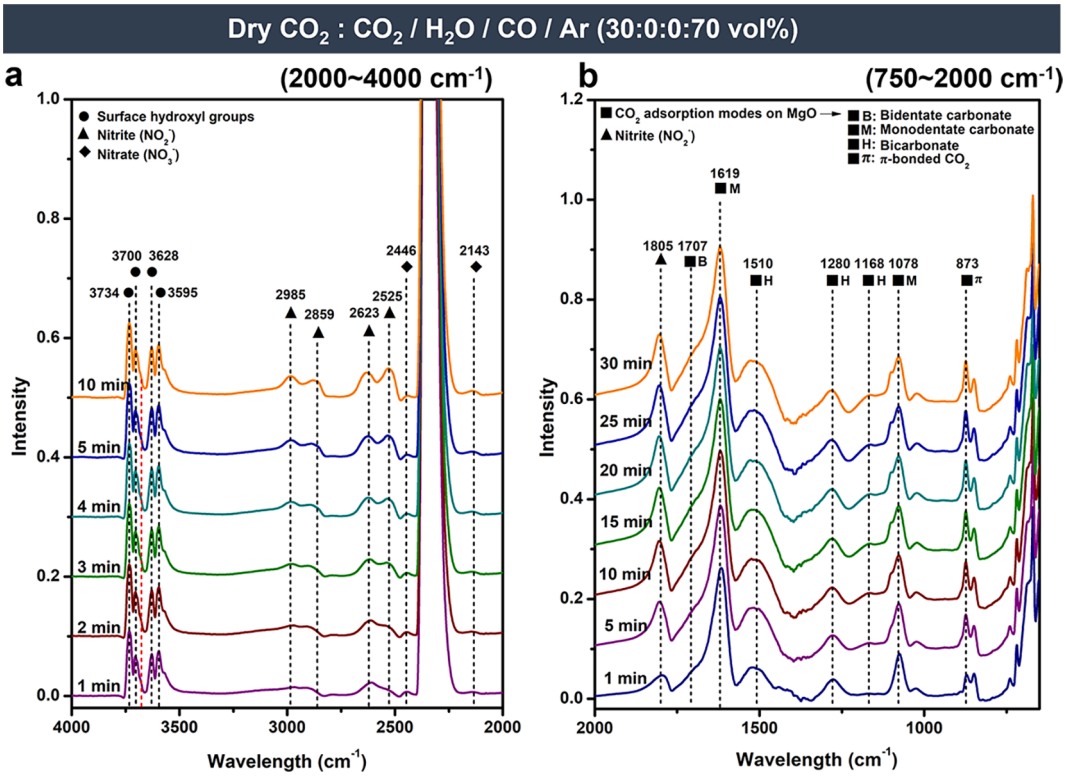

Fig. 3. *In situ* DRIFTS over salt-promoted $MgCeO_x$ sorbent at 300 °C, 1 bar, and 50 ml/min of Dry CO_2 feed in the range of (a) 2000 to 4000 cm^{-1} and (b) 750 to 2000 cm^{-1}.

detection was started, the time was set as 0 sec. The breakthrough time was considerably prolonged at higher total pressure. The breakthrough times at 1, 3, 6, and 10 bar were 164, 357, 766, and 1534 sec, respectively, as presented in the inset of Fig. 2(a). Therefore, higher pressure can contribute to the enhancement of the CO_2 sorption capacity and/or kinetics.

For the pre-combustion CO_2 capture, a certain level of CO inevitably remains in the feed stream. Breakthrough results under wet CO_2 feed conditions containing different CO concentrations at 10 bar are presented in Fig. 2(b). In the absence of CO at 10 bar, the breakthrough time was significantly delayed to 1534 sec, in comparison to the breakthrough time at 1 bar (164 sec). However, when CO was present in the feed gas, CO_2 was detected immediately regardless of the CO concentration. After the breakthrough curve gradually grew with time, it started to increase rapidly at the time when CO_2 became detectable in the test under CO-free wet feed gas (the inset of Fig. 2(b)). The shape of the breakthrough curves for the CO-containing feeds became wider with time. In addition to the reduction in CO_2 sorption capacity caused by the presence of CO, these results also indicated that CO molecules might preoccupy the strong sorption sites instead of the CO_2 molecules.

The breakthrough results showed that CO_2 sorption performance of the salt-promoted $MgCeO_x$ was enhanced by H_2O and interfered by CO. It is essential to understand the effects of these molecules on the CO_2 sorption mechanism to develop advanced MgO-based sorbents. Hereafter, underlying sorption mechanisms influenced by H_2O and CO molecules are proposed based on *in situ* DRIFTS analyses with various CO_2 mixtures (Table 2).

3.2. *In situ DRIFTS: Surface species induced by CO_2 sorption*

To identify the possible surface species resulting from only CO_2 sorption, the spectra obtained in the absence of non-target gas species (Dry CO_2 feed condition) were presented in Fig. 3. A band in the range of 2200–2400 cm^{-1} was commonly observed in all DRIFTS data at different

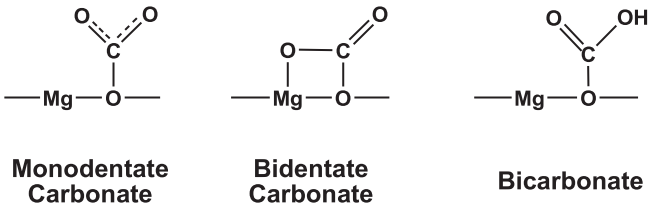

Scheme 1. Structure of carbonate complexes formed on MgO surface.

conditions, resulting from gaseous CO_2 [32]. The evolved peaks (square symbols) at 750–2000 cm^{-1} are mainly attributed to the carbonate species. Based on the peaks observed in this range, CO_2 is likely to be adsorbed in three forms, as presented in Scheme 1. The peak (square B) at 1707 cm^{-1} can be attributed to the bidentate carbonate species [33]; the peaks (square M) at 1078 cm^{-1} [34,35] and 1619 cm^{-1} [33,36,37] can be attributed to monodentate carbonate species. The bands (square H) at 1168–1510 cm^{-1} correspond to the bicarbonate species [36]; those at 1168 and 1280 cm^{-1} are ascribed to the C-OH bending mode, whereas the peaks at 1510 cm^{-1} can be assigned to the symmetric O-C-O stretching of bicarbonate species. The peak (square π) at 873 cm^{-1} represents the π-bonding of CO_3^{2-} in $MgCO_3$ formed upon CO_2 sorption [34].

In addition, spectra shown in DRIFTS figures revealed bands (triangle symbols) corresponding to nitrite (NO_2^-) at 1805 cm^{-1} and in the 2446–2985 cm^{-1} range, which has been proposed as an intermediate in the CO_2 sorption by the alkali metal nitrates salt-promoted MgO sorbent [22]. Peaks for nitrate (NO_3^-) were also observed (diamond symbols) at 2143 cm^{-1} and 2446 cm^{-1}; however, their intensities were weaker than those of the nitrite peaks. This result indicated that molten nitrate salts contributed to CO_2 sorption by dissociated into nitrite and O^{2-} ions. The bands (circle symbols) in the 3595–3734 cm^{-1} range can be attributed to the surface hydroxyl groups (OH groups) on the salt-promoted $MgCeO_x$.

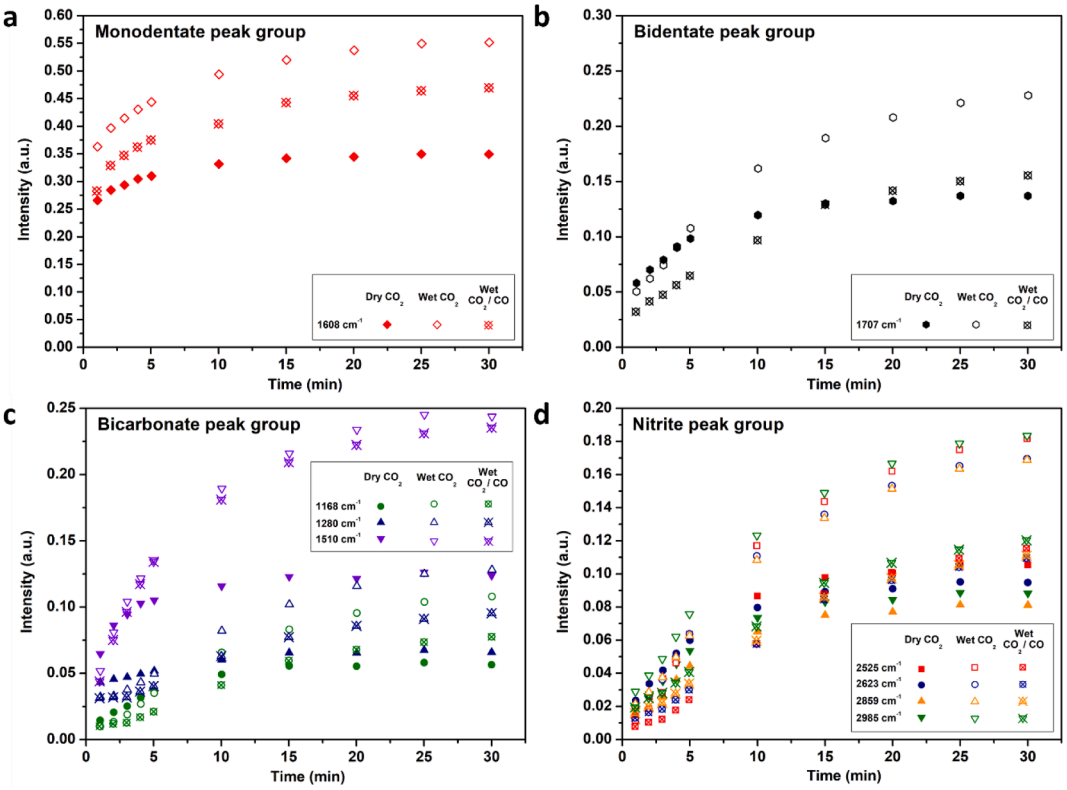

Fig. 4. Variation in peak intensities of the (a) monodentate carbonate group, (b) bidentate carbonate group, (c) bicarbonate group, and (d) nitrite group in *in situ* DRIFTS obtained under different feed compositions (Figs. 3 and S5).

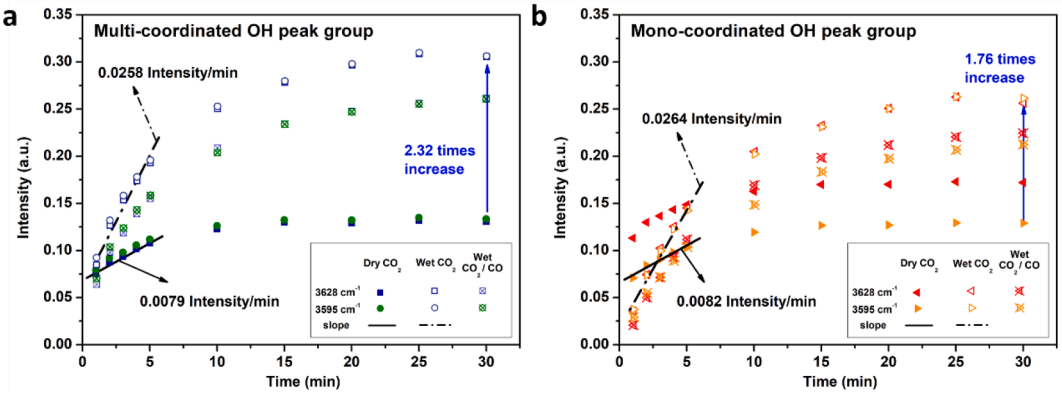

Fig. 5. Variation in peak intensities of (a) multi-coordinated surface OH group and (b) mono-coordinated surface OH group in *in situ* DRIFTS obtained under different feed compositions (Figs. 3 and S5).

The OH groups can be classified into multi-coordinated species at low wavelengths (~3674 cm^{-1}) and mono-coordinated species at high wavelengths over 3674 cm^{-1} [23,38]. This result indicated that CO_2 sorption changes the surface structure and results in the formation of both mono and multi-coordinated OH.

In the Dry CO_2 condition (Fig. 3), the evolution of monodentate carbonate peaks was most pronounced compared to other carbonate species, indicating that monodentate carbonate is the main product of CO_2 sorption on the surface of the salt-promoted $MgCeO_x$. Although no water was present in the dry feed condition, the peak intensities of bicarbonate species increased over the course of time. The observation of OH groups in the Dry CO_2 condition is possibly related to the aforementioned evolution of bicarbonate species. Accordingly, it could be concluded that CO_2 sorption leads to not only the formation of carbonate species, but also the transformation of the surface OH groups.

3.3. Promoted or interfered CO_2 sorption by non-target gas species, H_2O or CO

The mechanistic study on CO_2 sorption in the presence of non-target gas species was conducted by comparing the spectra obtained in the Dry CO_2 condition (Fig. 3(a-b)) with the spectra recorded under Wet CO_2, and Wet CO_2/CO conditions (Fig. S5(a-b) and Fig. S5(c-d)). In the presence of H_2O and/or CO in the feed gas, all the characteristic peaks observed in the Dry CO_2 condition were also observed, as shown in Fig. S5(a–d). However, their intensities were different, depending on the feed composition. For a clearer comparison, the peaks for carbonate species (monodentate carbonate, bidentate carbonate, bicarbonate), surface OH groups, and nitrite were isolated from Figs. 3 and S5, and their intensities were compared among the three different feed conditions (Dry CO_2, Wet CO_2, and Wet CO_2/CO), as shown in Fig. 4(a–d) and

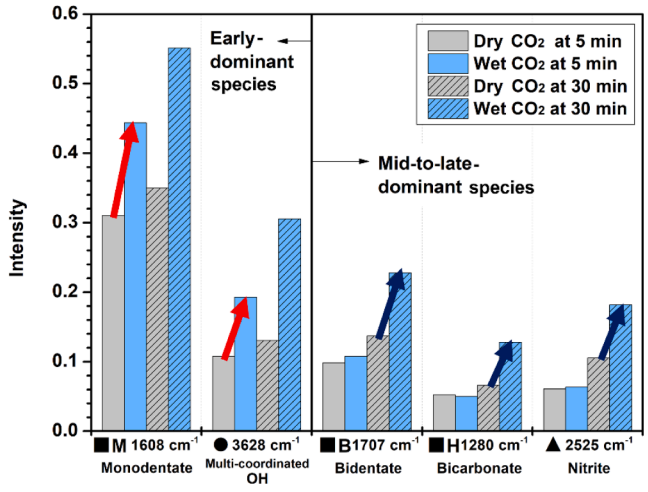

Fig. 6. Variation of intensities with time in Dry CO_2 and Wet CO_2 conditions.

Fig. 5(a–b).

Fig. 4(a, b, and c) indicate that all the peaks for carbonate species observed in the Wet CO_2 condition (blank symbols) and Wet CO_2/CO condition (blank × symbols) evolved faster and became larger than those in the Dry CO_2 condition (solid symbols). The peak evolution in the Wet CO_2/CO condition was smaller than that in the Wet CO_2 condition. As shown in Fig. 4(d), the formation of nitrite species was also enhanced in the Wet CO_2 condition (blank symbols), whereas this enhancement was reduced in the presence of CO (blank × symbols). More specifically, the intensities of monodentate peak in the wet conditions were higher during the entire sorption process compared to those in the Dry CO_2 condition (Fig. 4(a)). On the other hand, the intensities of bidentate peaks and bicarbonate peaks in the Wet CO_2 condition during the initial regime (5 min) were almost the same as those in the Dry CO_2 condition. Therefore, it could be concluded that H_2O in the feed gas contributed to enhancement of CO_2 sorption capacity and rate, while CO in the feed gas inhibited the CO_2 sorption from the beginning of the sorption. The facilitated formation of carbonate species in Wet CO_2 conditions was consistent with the extended breakthrough time, shown in Fig. 1(b), whereas the inhibition by CO could be also confirmed from Fig. 2(b).

The formation of surface OH groups was also inhibited by the presence of CO (Fig. 5(a-b)), as observed in carbonate and nitrite species (Fig. 4). In order to investigate the cause of the reductions in peak intensities, additional DRIFTS analyses and breakthrough experiments were performed in the Wet CO condition. The experimental results and the underlying mechanism of the CO-induced interference process is described after the discussion on the mechanism for the enhanced sorption in wet conditions.

From the rear wavelength range (2000–4000 cm^{-1}) shown in Fig. 5 (a-b), the effect of water vapor presence on the surface OH groups was observed. In the Wet CO_2 condition, the peaks corresponding to multi-coordinated OH groups were more pronounced than those in the Dry CO_2 condition, as presented in Fig. 5(a). The formation rates for the multi-coordinated OH group within the initial 5 min were 0.0079 and 0.0258 intensity/min for the Dry CO_2 and Wet CO_2 conditions, respectively, whereas the corresponding values for the mono-coordinated OH group were 0.0082 and 0.0264 intensity/min, respectively. After steady-state operation for 30 min, the peak intensity of the multi-coordinated OH group increased by 2.32 times in the Wet CO_2 condition compared to that in the Dry CO_2 condition, whereas the mono-coordinated OH group's peak intensity increased by 1.76 times. These results revealed that, in the presence of H_2O, the formation of multi-coordinated OH groups was preferentially promoted over mono-coordinated OH groups, in terms of both rate and total amount.

The formation mechanism of each surface OH group in $MgCeO_x$ can be illustrated by the existence of defects. Both types of OH groups can be generated by the dissociation of the supplied H_2O into OH and H at the defect sites on the surface of the $MgCeO_x$ [23], as shown in Scheme S1. The preferential promotion of multi-coordinated OH group than mono-coordinated OH group means dissociated OH was mainly located at an oxygen vacancy (O_v site). Therefore, the promotion of sorption in the

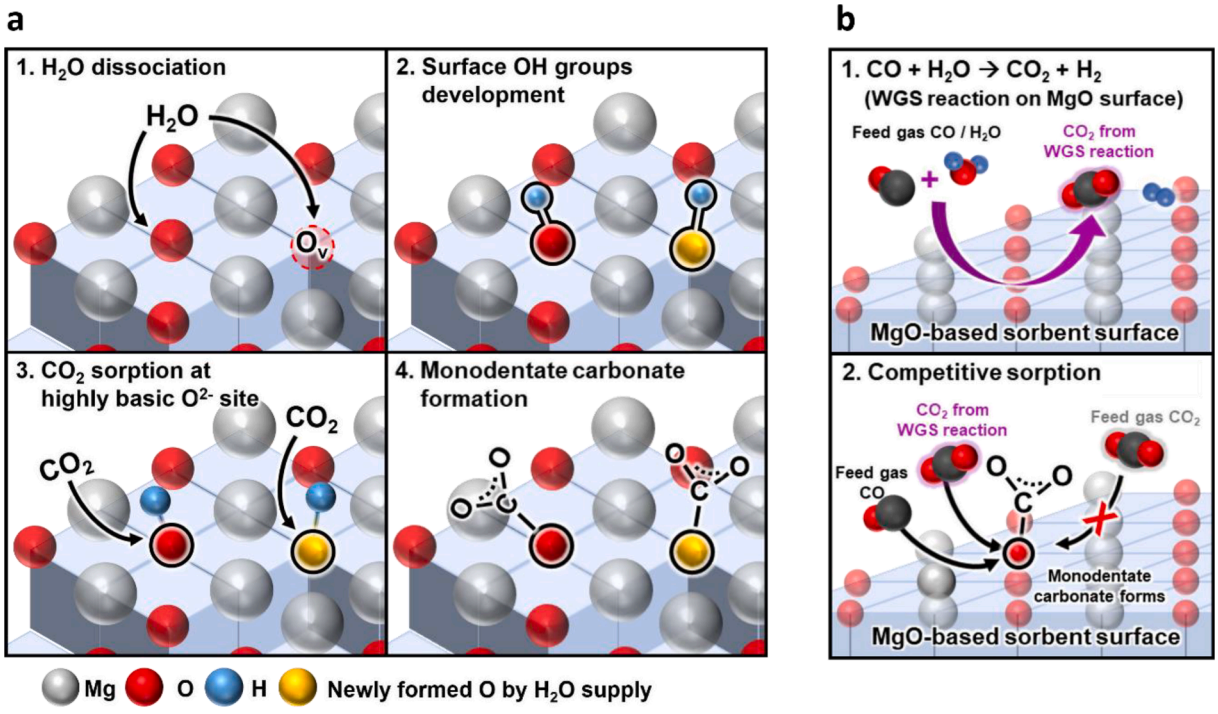

Scheme 2. Schematics of (a) CO_2 sorption mechanism during the early stages of sorption in Wet CO_2 condition and (b) mechanism of competitive CO_2 sorption induced by CO in Wet CO_2/CO condition on the surface of MgO-based sorbent.

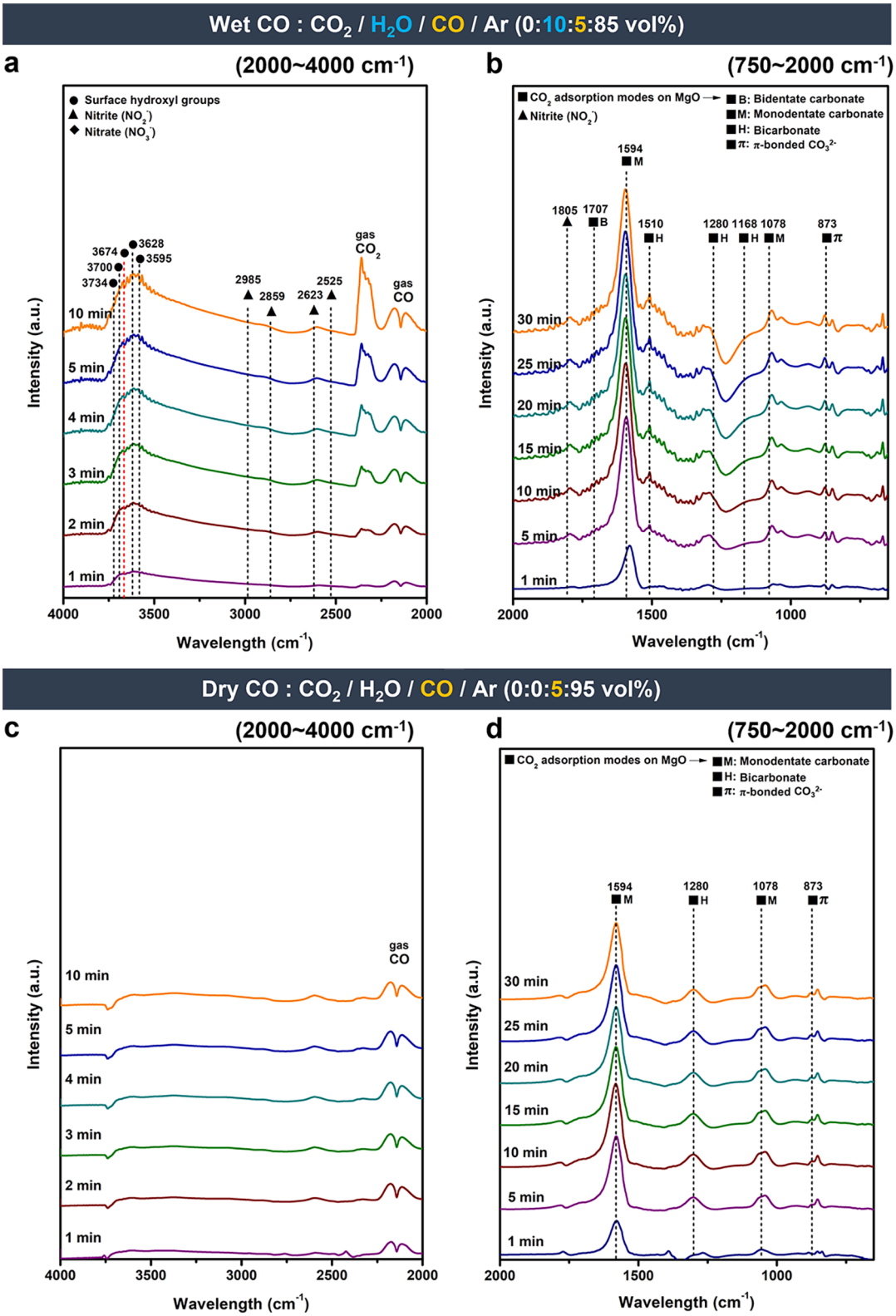

Fig. 7. *In situ* DRIFTS for salt-promoted $MgCeO_x$ sorbents at 300 °C, 1 bar, and 50 ml/min in (a-b) Wet CO and (c-d) Dry CO conditions.

presence of H_2O can be enhanced in the oxygen defect-abundant MgO-based sorbents.

In order to investigate the main contributor to the enhanced CO_2 capture performance by H_2O molecules, peaks exhibiting similar variance trends during early and mid-to-late regime, *i.e.,* 5 and 30 min, are summarized in Fig. 6. In the case of surface OH groups and monodentate carbonates, significant difference in the peak intensity between the Dry CO_2 and Wet CO_2 conditions was observed in the initial 5 min. Therefore, these two species were classified as early-dominant species. These results suggest that these early-dominant species likely affect the early stage of CO_2 sorption, which corresponded to the prolonged breakthrough time for the Wet CO_2 condition, shown in Fig. 1(b). Based on

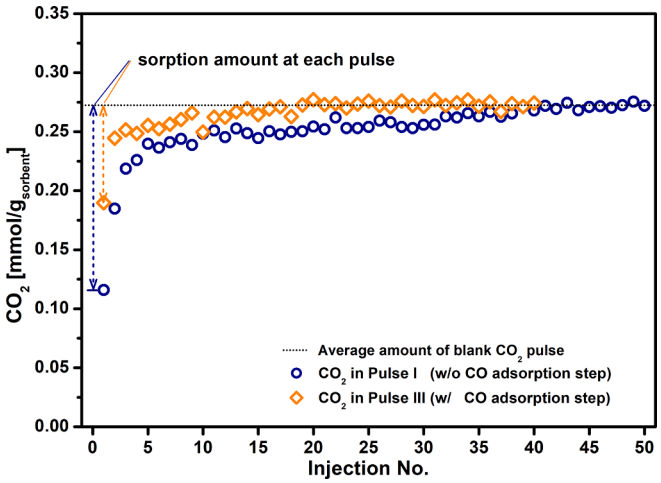

Fig. 8. CO_2 pulse titration experiments for salt-promoted $MgCeO_x$ sorbent at 300 °C with (Pulse III) and without (Pulse I) CO adsorption step. The titration was terminated when the amount of CO_2 detected reached the injected CO_2 amount in a blank test.

these results, the mechanism of CO_2 sorption at early stages can be illustrated, as depicted in Scheme 2(a). When the feed gas contained H_2O, the dissociation of H_2O initially created surface OH groups at the defects on the MgO surface at a fast rate (Steps 1 and 2). Thereafter, the resulting OH groups known to contain highly basic O^{2-} [39], could promote the formation of monodentate carbonate, as reported in the literature (Steps 3 and 4) [40,41]. Mediated by these highly basic OH groups, CO_2 sorption rate can be promoted in the early stages.

In contrast, nitrite, bidentate carbonate, and bicarbonate exhibited no meaningful differences within the initial 5 min. However, considerable difference was observed after 30 min (Mid-to-late-dominant species, shown in Fig. 6). This observation was consistent with that the carbonation by the molten nitrate salts results in bidentate carbonate and bicarbonate [42]. Therefore, the sorption mechanism involving molten nitrated salts contributed to CO_2 capture after the early time regime, leading to the relatively less steep slopes of the breakthrough curves.

The interference of CO on the CO_2 sorption was further studied by conducting breakthrough experiments, pulse titration experiments and the DRIFTS analysis in the Wet CO condition without CO_2 (Table 2). In both *in situ* DRIFTS (Fig. 7(a)) and the breakthrough experiment (Fig. S6), CO_2 was detected as a product, even in the absence of CO_2 in the feed gas. On the other hand, it was noted that CO_2 was not generated in the absence of H_2O (Fig. 7(c)). Thus, the simultaneous detection of H_2 with CO_2 in the breakthrough experiment (Fig. S6) demonstrated that the WGS reaction occurred at the surface of the salt-promoted $MgCeO_x$ [43], as described in Step 1 of Scheme 2(b). The result indicated that carbonate peaks in Fig. 7(a) resulted from either the sorption of CO_2 produced by the WGS reaction or adsorption of fed CO.

The appearance of the monodentate carbonate in Dry CO condition supported that CO was adsorbed on the surface of the salt-promoted $MgCeO_x$. To confirm whether the sites occupied by CO adsorption were identical to the sites for CO_2 adsorption, the pulse titration was conducted by injecting 300 ul of CO or CO_2 for multiple times because it could consequently elucidate the CO_2 sorption hampered by CO adsorption (Fig. 8). In the Pulse I experiment where CO_2 was directly injected without any treatment for sorbent, approximately half of injected CO_2 (0.152 mmol/$g_{sorbent}$) was sorbed at the first injection and the amount of sorbed CO_2 gradually decreased. For comparison, the salt-promoted $MgCeO_x$ was initially subjected to the CO pulse titration for CO adsorption. After He purge, subsequent CO_2 pulse titration (Pulse III) was followed. As shown in Fig. 8, the amount of sorbed CO_2 decreased to 0.078 mmol/$g_{sorbent}$ at the first injection compared to the sorbed CO_2 amount without CO pre-adsorption. The difference in CO_2 sorption amount was observed up to 35 injections. The result suggested that CO pre-occupied the site where CO_2 could be sorbed via competitive sorption.

As a result of both CO adsorption and CO_2 sorption produced by the WGS reaction, the monodentate carbonate (square M) was immediately formed as shown in Fig. 7(b) and Fig. 7(d). It implied that early-dominant species, *i.e.,* monodentate carbonate, dominated over the other carbonate peaks (square B, H) throughout the entire sorption process. As depicted in Step 2 of Scheme 2(b), this result indicated that the competitive sorption among CO_2 in the feed gas, WGS reaction-induced CO_2, and CO causes a deterioration in the initial rate and performance of CO_2 sorption. The breakthrough of CO_2, which occurs from the beginning of the process in the presence of CO (insert in Fig. 2(b)), can be explained by the pre-occupied CO_2 sorption sites in the same manner.

The nitrite (triangle symbols) was obtained from the transformation of nitrate ions to a very small extent in both the Wet CO and Dry CO conditions (Fig. 7(a) and Fig. 7(c)). This result indicates that the aforementioned molten nitrate salts-involved-CO_2 sorption process did not proceed as much as in the absence of CO. Following the nitrate peaks, bicarbonate (square H) and bidentate carbonate (square B) peaks, which were classified as the dominant species during the mid-to-late regime, exhibited a similar tendency for all feed conditions containing CO (Fig. S5(c–d) and Fig. 7). These results were also consistent with the breakthrough curves becoming less steep as the CO content was increased, as shown in Fig. 2(b).

Based on these DRIFTS results, it was concluded that H_2O enhances the initial CO_2 sorption kinetics of $MgCeO_x$, and the sorption proceeds mainly to form monodentate carbonate. Furthermore, the CO-induced interference occurs through the following two mechanisms: (i) the competitive sorption between CO_2 from the feed gas versus WGS-induced CO_2 and CO during the initial sorption step, and (ii) deactivation of the molten nitrate salts-involved-CO_2 sorption process in the mid-to-late regime.

4. Conclusions

This study provides insights into the CO_2 sorption mechanism of MgO-based sorbents in the presence of H_2O and CO, which is inevitable in the effluent gas for pre-combustion CO_2 capture. The results for the CO_2 sorption performance indicated that the composition of the feed gas is a dominant factor in determining the dynamic CO_2 sorption behavior. In contrast, the temperature does not significantly affect the breakthrough performance in the tested temperature range. Additionally, the DRIFTS analyses provided an understanding of the mechanism underlying the phenomena observed in the breakthrough tests.

In wet conditions, the breakthrough time increased significantly from 159 sec to 213 sec as the H_2O content was increased from 0 to 60 % along with 30 % CO_2. Furthermore, the DRIFTS peak intensities of multi-coordinated and mono-coordinated OH groups in wet conditions increased by 2.32 and 1.72 times, respectively, compared to that in dry conditions. These results indicated that the surface OH groups were developed by the dissociation of H_2O at the oxygen vacancies on the $MgCeO_x$ surface, which were subsequently occupied by the OH groups. In particular, the peak intensities of adsorbed OH groups and monodentate carbonate in wet conditions increased at remarkably high rates compared to other surface species. The result suggested that H_2O may function as a crucial component in the initial rapid sorption of CO_2, allowing CO_2 to be bound in the form of monodentate carbonate. CO_2 sorption in the mid-to-late regime is mediated by alkali metal salts, which is accompanied by the formation of the nitrite ions, bidentate carbonate, and bicarbonate.

Even under wet conditions, the presence of CO results in the immediate breakthrough of a trace amount of CO_2 in the fixed bed test and decreases the CO_2 sorption capacity of the sorbents. This interrupted

CO_2 sorption in the co-existence of CO and H_2O was caused by competitive sorption. First, the WGS reaction was catalyzed by $MgCeO_x$ to generate CO_2. Then, CO and the WGS-induced CO_2 occupy the sorption sites where CO_2 in the feed gas could be sorbed, thereby hindering initial rapid CO_2 sorption. Furthermore, the presence of CO deteriorates CO_2 sorption driven by molten nitrate salts, decreasing the CO_2 sorption capacity in the mid-to-late regime.

To understand and evaluate the dynamic sorption behavior of sorbents in the practically relevant conditions, it is essential to study sorption mechanisms in the presence of polar molecules such as H_2O and CO. The results in this study provide guidance to determine the priority for obstacles to be overcome for the ultimate application of MgO-based sorbents.

Declaration of Competing Interest

The authors declare that they have no known competing financial interests or personal relationships that could have appeared to influence the work reported in this paper.

Acknowledgments

This work was supported by the National Research Foundation of Korea (NRF), funded by the Ministry of Science and ICT (2019K1A4A7A03113187).

Appendix A. Supplementary data

Supplementary data to this article can be found online at https://doi.org/10.1016/j.cej.2022.134607.

References

[1] International Energy Agency (IEA), Paris, Energy Technology Perspectives 2020 (2020). https://www.iea.org/reports/energy-technology-perspectives-2020.
[2] M. Bui, C.S. Adjiman, A. Bardow, E.J. Anthony, A. Boston, S. Brown, P.S. Fennell, S. Fuss, A. Galindo, L.A. Hackett, Carbon capture and storage (CCS): the way forward, Energ. Environ. Sci. 11 (5) (2018) 1062–1176.
[3] A.Ö. Yazaydın, R.Q. Snurr, T.-H. Park, K. Koh, J. Liu, M.D. LeVan, A.I. Benin, P. Jakubczak, M. Lanuza, D.B. Galloway, J.J. Low, R.R. Willis, Screening of metal–organic frameworks for carbon dioxide capture from flue gas using a combined experimental and modeling approach, J. Am. Chem. Soc. 131 (51) (2009) 18198–18199.
[4] Y.G. Chung, D.A. Gómez-Gualdrón, P. Li, K.T. Leperi, P. Deria, H. Zhang, N. A. Vermeulen, J.F. Stoddart, F. You, J.T. Hupp, O.K. Farha, R.Q. Snurr, In silico discovery of metal–organic frameworks for precombustion CO_2 capture using a genetic algorithm, Sci. Adv. 2 (10) (2016), https://doi.org/10.1126/sciadv.1600909.
[5] D. Jansen, M. Gazzani, G. Manzolini, E. van, Pre-combustion CO_2 capture, Int. J. Greenh. Gas. Con. 40 (2015) 167–187.
[6] B. Metz, O. Davidson, H.D. Coninck, M. Loos, L. Meyer, IPCC special report on carbon dioxide capture and storage, Cambridge University Press, 2005. Chapter 3.
[7] S. Lian, C. Song, Q. Liu, E. Duan, H. Ren, Y. Kitamura, Recent advances in ionic liquids-based hybrid processes for CO_2 capture and utilization, J. Environ. Sci. 99 (2021) 281–295.
[8] A. Mutch, S. Shulda, A.J. McCue, M.J. Menart, C.V. Ciobanu, C. Ngo, J. A. Anderson, R.M. Richards, D. Vega-Maza, Carbon capture by metal oxides: unleashing the potential of the (1 1 1) facet, J. Am. Chem. Soc. 140 (13) (2018) 4736–4742.
[9] S. Jin, K.-J. Ko, C.-H. Lee, Direct formation of hierarchically porous MgO-based sorbent bead for enhanced CO_2 capture at intermediate temperatures, Chem. Eng. J. 371 (2019) 64–77.
[10] S.J. Park, Y. Kim, C.W.J.C. Jones, $NaNO_3$ Promoted Mesoporous MgO for High Capacity CO_2 Capture from Simulated Flue Gas with Isothermal Regeneration, Chem. Sus. Chem. 13 (2020) 2988–2995.
[11] P. Liu, P.M. Abdala, G. Goubert, M.G. Willinger, C. Copéret, Ultrathin single crystalline MgO(1 1 1) nanosheets, Angew. Chem. Int. Edit. 60 (2021) 3254–3260.
[12] Y. Hu, Y. Guo, J. Sun, H. Li, W. Liu, Progress in MgO sorbents for cyclic CO_2 capture: a comprehensive review, J. Mater. Chem. A 7 (35) (2019) 20103–20120.
[13] T. Harada, T.A. Hatton, Colloidal nanoclusters of MgO coated with alkali metal nitrates/nitrites for rapid, high capacity CO_2 capture at moderate temperature, Chem. Mater. 27 (23) (2015) 8153–8161.
[14] H. Lee, M.L.T. Triviño, S. Hwang, S.H. Kwon, S.G. Lee, J.H. Moon, J. Yoo, J.G. Seo, *In situ* observation of carbon dioxide capture on pseudo-liquid eutectic mixture-promoted magnesium oxide, ACS Appl. Mater. Interfaces. 10 (3) (2018) 2414–2422.
[15] K. Kwapien, J. Paier, J. Sauer, M. Geske, U. Zavyalova, R. Horn, P. Schwach, A. Trunschke, R. Schlögl, Sites for methane activation on lithium-doped magnesium oxide surfaces, Angew. Chem. Int. Edit. 53 (2014) 8774–8778.
[16] G. Xiao, R. Singh, A. Chaffee, P. Webley, Advanced adsorbents based on MgO and K_2CO_3 for capture of CO_2 at elevated temperatures, Int. J. Green Gas Con. 5 (4) (2011) 634–639.
[17] A.-T. Vu, K. Ho, S. Jin, C.-H. Lee, Double sodium salt-promoted mesoporous MgO sorbent with high CO_2 sorption capacity at intermediate temperatures under dry and wet conditions, Chem. Eng. J. 291 (2016) 161–173.
[18] S. Jin, K. Ho, C.-H. Lee, Facile synthesis of hierarchically porous MgO sorbent doped with $CaCO_3$ for fast CO_2 capture in rapid intermediate temperature swing sorption, Chem. Eng. J. 334 (2018) 1605–1613.
[19] J. Ding, C. Yu, J. Lu, X. Wei, W. Wang, G.J.A.E. Pan, Enhanced CO_2 adsorption of MgO with alkali metal nitrates and carbonates, Appl. Energy. 263 (2020), 114681.
[20] K. Wang, Y. Zhao, P.T. Clough, P. Zhao, E.J.J. Anthony, Structural and kinetic analysis of CO_2 sorption on $NaNO_2$-promoted MgO at moderate temperatures, Chem. Eng. J. 372 (2019) 886–895.
[21] A. Dal Pozzo, A. Armutlulu, M. Rekhtina, P.M. Abdala, C.R. Müller, CO_2 Uptake and Cyclic Stability of MgO-Based CO_2 Sorbents Promoted with Alkali Metal Nitrates and Their Eutectic Mixtures, ACS Appl. Energy Mater. 2 (2) (2019) 1295–1307.
[22] H.A. Lara-García, W. Gao, A. Gómez-Cortés, G. Diaz, H. Pfeiffer, Q. Wang, High and efficient CO_2 capture in molten nitrate-modified Mg–Al–palmitate layered double oxides at high pressures and elucidation of carbonation mechanisms by *in situ* DRIFT spectroscopy analysis, Ind. Eng. Chem. Res. 58 (14) (2019) 5501–5509.
[23] S. Jin, Y. Park, G. Bang, N.D. Vo, C.-H. Lee, Revisiting magnesium oxide to boost hydrogen production via water–gas shift reaction: mechanistic study to economic evaluation, Appl. Catal. B 284 (2021) 119,701.
[24] Y. Qiao, J. Wang, Y. Zhang, W. Gao, T. Harada, L. Huang, T.A. Hatton, Q. Wang, Alkali Nitrates Molten Salt Modified Commercial MgO for Intermediate-Temperature CO_2 Capture: Optimization of the Li/Na/K Ratio, Ind. Eng. Chem. Res. 56 (6) (2017) 1509–1517.
[25] T. Binninger, B. Pribyl, A. Pătru, P. Ruettimann, S. Bjelić, T.J. Schmidt, Multivariate calibration method for mass spectrometry of interfering gases such as mixtures of CO, N_2, and CO_2, J. Mass Spectrom. 53 (12) (2018) 1214–1221.
[26] W. Gao, M.A. Vasiliades, C.M. Damaskinos, M. Zhao, W. Fan, Q. Wang, T.R. Reina, A.M. Efstathiou, Molten salt-promoted MgO adsorbents for CO_2 capture: Transient kinetic studies, Environ. Sci. Technol. 55 (2021) 4513–4521.
[27] W. Gao, J. Xiao, Q. Wang, S. Li, M.A. Vasiliades, L. Huang, Y. Gao, Q. Jiang, Y. Niu, B. Zhang, Y. Liu, H. He, A.M. Efstathiou, Unravelling the mechanism of intermediate-temperature CO_2 interaction with molten-$NaNO_3$-salt-promoted MgO, Adv. Mater. (2021), 2106677.
[28] L. Zhang, Y. Zheng, Y. Guo, S. Bai, M. Song, P. Huang, X. Wei, J. Sun, C. Li, J. Zhang, C. Zhao, Alkali metal nitrates promoted MgO composites with high CO_2 uptake for thermochemical energy storage, ACS Appl. Energy Mater. 4 (2021) 9513–9524.
[29] Y. Park, Y. Ju, D. Park, C.-H. Lee, Adsorption equilibria and kinetics of six pure gases on pelletized zeolite 13X up to 1.0 MPa: CO_2, CO, N_2, CH_4, Ar and H_2, Chem. Eng. J. 292 (2016) 348–365.
[30] C.H. Lee, K.B. Lee, Sorption-enhanced water gas shift reaction for high-purity hydrogen production: Application of a Na-Mg double salt-based sorbent and the divided section packing concept, Appl. Energy. 205 (2017) 316–322.
[31] P. Liu, X. Wang, X. Li, T. Zhang, G. Du, W. Liu, Competitive adsorption characteristics of CH_4/C_2H_6 gas mixtures on model substances, coal and shale, Fuel 279 (2020), 118038.
[32] J. Hu, K. Zhu, L. Chen, C. Kübel, R. Richards, MgO (1 1 1) nanosheets with unusual surface activity, J. Phys. Chem. C 111 (32) (2007) 12038–12044.
[33] M. Signorile, J.G. Vitillo, M. D'Amore, V. Crocellà, G. Ricchiardi, S. Bordiga, Characterization and Modeling of Reversible CO_2 Capture from Wet Streams by a MgO/Zeolite Y Nanocomposite, J. Phys. Chem. C 123 (28) (2019) 17214–17224.
[34] K. Nakamoto, Infrared and Raman spectra of inorganic and coordination compounds. Handbook of vibrational spectroscopy, John Wiley & Sons, 2006.
[35] D. Cornu, H. Guesmi, J.-M. Krafft, H. Lauron-Pernot, Lewis acido-basic interactions between CO_2 and MgO surface: DFT and DRIFT approaches, J. Phys. Chem. C 116 (11) (2012) 6645–6654.
[36] W. Gao, T. Zhou, Q. Wang, Controlled synthesis of MgO with diverse basic sites and its CO_2 capture mechanism under different adsorption conditions, Chem. Eng. J. 336 (2018) 710–720.
[37] P. Li, W. Liu, J.S. Dennis, H.C. Zeng, Synthetic architecture of MgO/C nanocomposite from hierarchical-structured coordination polymer toward enhanced CO_2 capture, ACS Appl. Mater. Interfaces 9 (11) (2017) 9592–9602.
[38] E. Knözinger, K.-H. Jacob, S. Singh, P. Hofmann, Hydroxyl groups as IR active surface probes on MgO crystallites, Surf. Sci. 290 (3) (1993) 388–402.
[39] J. Di Cosimo, V. Díez, C. Ferretti, C. Apesteguía, Basic catalysis on MgO: generation, characterization and catalytic properties of active sites, Catalysis 26 (2014) 1–28.
[40] J. Evans, T. Whateley, Infra-red study of adsorption of carbon dioxide and water on magnesium oxide, Trans. Faraday Soc. 63 (1967) 2769–2777.
[41] H. Petitjean, H. Guesmi, H.L.N. Lauron-Pernot, G. Costentin, D. Loffreda, P. Sautet, F. Delbecq, How surface hydroxyls enhance MgO reactivity in basic catalysis: the case of methylbutynol conversion, ACS Catal. 4 (11) (2014) 4004–4014.
[42] S. Kim, K.B. Lee, Impregnation of hydrotalcite with $NaNO_3$ for enhanced high-temperature CO_2 sorption uptake, Chem. Eng. J. 356 (2019) 964–972.
[43] S. Jin, H. Byun, C.-H. Lee, Enhanced oxygen mobility of nonreducible MgO-supported Cu catalyst by defect engineering for improving the water–gas shift reaction, J. Cat. 400 (2021) 195–211.